Chinese Journal of Mechanical Engineering

ORIGINAL ARTICLE

Open Access

Prediction of Grinding Force by an Electroplated Grinding Wheel with Orderly-Micro-Grooves

Cong Mao[1,4], Jiali Wang[1], Mingjun Zhang[1*], Xincheng Wang[2], Yuanqiang Luo[1], Weidong Tang[1], Kun Tang[1], Zhuming Bi[3], Yongle Hu[1] and Zhenheng Lin[4]

Abstract

The ability to predict a grinding force is important to control, monitor, and optimize the grinding process. Few theoretical models were developed to predict grinding forces when a structured wheel was used in a grinding process. This paper aimed to establish a single-grit cutting force model to predict the ploughing, friction and cutting forces in a grinding process. It took into the consideration of actual topography of the grinding wheel, and a theoretical grinding force model for grinding hardened AISI 52100 by the wheel with orderly-micro-grooves was proposed. The model was innovative in the sense that it represented the random thickness of undeformed chips by a probabilistic expression, and it reflected the microstructure characteristics of the structured wheel explicitly. Note that the microstructure depended on the randomness of the protruding heights and distribution density of the grits over the wheel. The proposed force prediction model was validated by surface grinding experiments, and the results showed (1) a good agreement of the predicted and measured forces and (2) a good agreement of the changes of the grinding forces along with the changes of grinding parameters in the prediction model and experiments. This research proposed a theoretical grinding force model of an electroplated grinding wheel with orderly-micro-grooves which is accurate, reliable and effective in predicting grinding forces.

Keywords Electroplated grinding wheel, Orderly-micro-grooves, Grinding force, Force prediction, Undeformed chip thickness, Experimental validation

1 Introduction

A grinding wheel can be structured to improve efficiency and reduce the burns in a grinding process. How to structure a grinding wheel for the improvement of the grinding process attracted a great deal of attention in both academic and industrial communities [1]. For example, Dewar et al. [2] made a grinding wheel with high-angle helical grooves, and experiments showed that the grinding efficiency was improved considerably. Xu et al. [3] introduced a grooved grinding disc for quality improvement in grinding cubic zirconia. Zhang et al. [4] tested the grinding performance of a macro-structured wheel and found it decreased the grinding temperature significantly. Denkena et al. [5] adopted a patterned structure in a grinding wheel to enhance the grinding performance by reducing grinding forces and burns. Kirsch and Aurich [6] investigated a slotted grinding wheel and found it improved the cooling efficiency in the grinding process. The authors in this paper structured

*Correspondence:
Mingjun Zhang
mj_zhang@csust.edu.cn
[1] Hunan Provincial Key Laboratory of Intelligent Manufacturing Technology for High-performance Mechanical Equipment, Changsha University of Science and Technology, Changsha 410114, China
[2] Hunan Wuxin Intelligence Technology Co., Ltd, Changsha 410199, China
[3] Department of Civil and Mechanical Engineering, Purdue University Fort Wayne, Fort Wayne, IN 46805, USA
[4] School of Mechanical and Electrical Engineering, Putian University, Putian 351100, China

the peripheral surface of a grinding wheel using a set of orderly-micro-grooves with 0.1 mm in width, 1.5 mm in depth, and 0.98 mm in interval [7]; it was used to grind silica glass to reduce grinding temperature and force. All of the aforementioned works revealed the fact that in comparison with a conventional grinding wheel, a structured grinding wheel with specific textures and patterns could reduce grinding force, grinding temperature and burns and thus improve overall grinding performance. However, few theoretical models were developed to predict grinding forces when a structured wheel was used in a grinding process.

In a grinding process, the surface quality, specific energy, grinding temperature and wheel wear are related greatly to the grinding force; therefore, the quality control of a grinding process requires the information of the grinding force. Conventionally, precision dynamometers are commonly used to measure grinding forces. Due to the complexity and additional cost of physical measurements, it is significantly beneficial to develop theoretical models to predict grinding forces; especially, when different structures of a grinding wheel are taken into consideration.

To model a grinding process, physical interactions between individual grits and the workpiece are first investigated and are then expanded to model the behavior of the whole grinding wheel [8]. The probabilistic distribution of grits on the wheel surface makes the grinding process random, and then the chips are generated stochastically, and so are the thicknesses of the undeformed chips. Note that the grinding force depends on the thickness of the undeformed chip. Kadivar et al. [9] established a grinding force prediction model with the assumption of the random thickness distribution of undeformed chips. The force prediction models by Ma et al. [10] and Ni et al. [11] emphasized on random distributions and protruding heights of grits over the wheel, respectively. Chang and Wang [12] adopted a stochastic density function to describe the random distribution of grits over the grinding wheel, and a dynamic grinding force model was presented. Agarwal and Rao [13] used a probability density function to represent the randomness of chip thicknesses in their grinding force model. Dai et al. [14] assumed that the probabilistic distribution of undeformed chip thickness depended on the kinematic conditions, material properties, wheel microstructure, and dynamic effects. Cheng and Gong [15] analyzed the undeformed chip thickness of single-crystal silicon and developed a grinding force prediction model with the consideration of the crystallographic effect in microgrinding. The grinding force predicted by Li et al. [16] was determined by the strain rate, the randomly distributed radii of grits, and the depth of elastic-to-plastic transition.

Numerous factors that affected a grinding force were analyzed by different researchers. Durgumahanti et al. [17] investigated the friction and ploughing forces in a grinding process and concluded that the ploughing force contributed to the grinding force significantly. The grinding force model by Ardashevdv and Dyakonov [18] considered different wear mechanisms of grits. Liu et al. [19] discussed the effect of an impact load on the grinding force. Zhang et al. [20] established a theoretical grinding force model by taking into account three grinding stages, i.e., ductile-stage, ductile-to-brittle-transition-stage and brittle-stage. On the other hand, Sun et al. [21] presented a grinding force model by considering three primary grinding force components, inducing the ductile removal force, the brittle removal force and the frictional force. Similarly, Zhou et al. [22] proposed to decompose a grinding force into the components of chip formation force, frictional force, and fracture force. Xiao et al. [23] proposed a grinding force model for gear profile grinding by taking into account rubbing, plowing and cutting. Li et al. [16] analyzed the grinding force components and grinding trajectory based on the critical depth of rubbing, ploughing, and brittle fracture. Zhang et al. [24] discussed the effects of cutting, stacking, ploughing mechanisms on the grinding force. Xiao et al. [25] modeled the grinding forces in the ductile and brittle zones, respectively. Jamshidi et al. [26] proposed an analytical force model based on the assumed kinematic-geometrical relations. Werner [27] estimated the grinding force by considering the combined effect of friction and chip formation. In the surface grinding force model by Tang et al. [28], average contact pressure and friction coefficient were considered as two main process variables. Malkin and Guo [29] developed a force prediction model from the perspective of energy conservation by taking into account sliding energy, ploughing energy and strain energy in chip formation.

This paper aimed to develop a grinding force prediction model by an electroplated grinding wheel with orderly-micro-grooves; moreover, the randomness of the protruding heights and distribution of the grits would be specially considered. The cutting force of a single grit and the effect of the structured micro-grooves on the grinding force were estimated. Experiments were designed to validate the accuracy, reliability, and effectiveness of the proposed grinding force prediction model.

2 Grinding Force Model

2.1 Chip Thickness Model

A grinding process is characterized by multi-point cutting where multiple cutting edges with a large negative rake angle are engaged to remove tiny chips with a very high plastic strain rate. Since the grits over a grinding

wheel exhibit the randomness of the distribution and protruding heights, the thicknesses of chips are formed randomly, and it is critical to understand the chip formation mechanisms in predicting grinding forces.

The thicknesses of chips depend on a number of factors including the geometry of grits, the process parameters, and the material properties of the workpiece and the cutting tool. To develop a concise force prediction model with the consideration of main design factors, the following assumptions were made at the interfaces of grits and workpiece: (1) based on the observations over a grinding wheel by a 3D ultra-depth of field microscope, the grits were modeled by a conic shape with a flatted tip. (2) The protruding heights of grits were randomly distributed, and correspondingly, the cutting depths of individual grits and the thicknesses of chips were distributed randomly. A Rayleigh probability density function (P.D.F.) by Hecker [8] could be used to represent the distribution of the protruding heights of grits. Therefore, the spectrum of chip thickness generated is assumed to have the same mathematical distribution. (3) The profile of the scratches on the workpiece by individual grits is the same and completely defined by the depth of engagement or undeformed chip thickness h.

The relative motion of grit over the workpiece surface generates a removed chip with a curved longitudinal shape, as shown in Figure 1. The thickness over a chip varied from zero to a maximum value of h_m; the cross-section geometry of the chip was determined by that of the conical grit.

To model the randomness of undeformed chip thickness h, the Rayleigh probability density function $f(h)$ [8] is used.

$$f(h) = \begin{cases} (h/\delta^2)e^{-\frac{h^2}{2\delta^2}}, & h \geq 0, \\ 0, & h < 0, \end{cases} \tag{1}$$

where h is the undeformed chip thickness, and it is the actual engagement depth between individual grit and the workpiece. δ is a constant for the Rayleigh P.D.F. that depended on the cutting conditions, microstructure of grinding wheel, the material properties of workpiece. The Rayleigh distribution is determined by its unique parameter δ.

The expected value $E(h)$ of the above function is expressed by

$$E(h) = \int_0^\infty hf(h)\mathrm{d}h = \sqrt{\frac{\pi}{2}}\delta. \tag{2}$$

With the assumption of a grit with conic shape, the expected cross-section area $E(A_{ch})$ of a single-chip can be further determined by

$$E(A_{ch}) = \frac{\pi}{2}E\left(h^2\right). \tag{3}$$

The expected total engagement area of N_d number of active grits is determined on the projection plane that is perpendicular to the grit movement trajectory of the grinding wheel as

$$E(A_{total}) \approx N_d E(A_{ch}) = N_d \frac{\pi}{2} E\left(h^2\right). \tag{4}$$

The number N_d of active grits in the grinding zone is determined by

$$N_d = \int_0^{l_c} bC_d\mathrm{d}l = bl_cC_d, \tag{5}$$

where l_c is the arc length of actual wheel-workpiece contact, b is the grinding width, and C_d is the number of active grits per unit area.

Since the mass and volume of plastically deformed materials were conserved, the material removal rate can be calculated from the total engagement area of grits $E(A_{total})$ and the wheel velocity v_s as

$$E(A_{total})v_s = ba_pv_w, \tag{6}$$

where v_w is the workpiece velocity, and a_p is the grinding depth.

Using Eqs. (3) and (4) yielded the dependence of the chip thickness h on the main process parameters in grinding as

$$E\left(h^2\right) = \frac{2ba_pv_w}{\pi N_d v_s} = \frac{2a_pv_w}{\pi l_c C_d v_s}. \tag{7}$$

Note that the left side of Eq. (7) can be calculated according to the Rayleigh distribution

$$E\left(h^2\right) = \int_{h_{cr}}^\infty h^2\bar{f}(h)\mathrm{d}h = 2\delta^2 + h_{cr}^2, \tag{8}$$

where h_{cr} is the critical thickness of undeformed chip; it is calculated as $h_{cr} = r \cdot [1 - \cos(\alpha)]$. α is a stagnation angle in the range of 44°~63°, and its default value is 55° [30]. r is the grit radius, and $\bar{f}(h)$ is a redefined P.D.F. of the

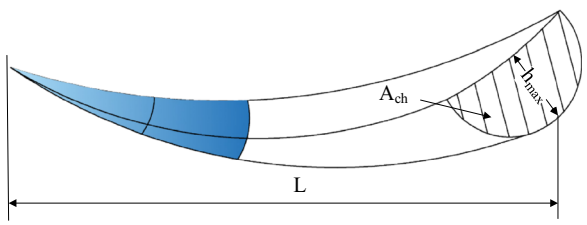

Figure 1 Single-chip in its undeformed state

average chip thickness. Note that $r \geq 0$ since a chip is possibly formed only when the grit cut into the workpiece to a critical depth. Furthermore, it is proposed to rescale the original P.D.F. by a new function of $\int_{h_{cr}}^{\infty} \overline{f}(h)\mathrm{d}h = 1$.

Combining Eqs. (7) and (8) yielded the parameter δ of the Rayleigh density function as

$$\delta = \sqrt{\frac{a_p v_w b}{\pi N_d v_s} - \frac{h_{cr}^2}{2}}. \tag{9}$$

Finally, combining Eqs. (2) and (9) get the undeformed chip thickness as

$$E(h) = \sqrt{\frac{a_p v_w b}{2N_d v_s} - \frac{\pi h_{cr}{}^2}{4}}. \tag{10}$$

2.2 Cutting Force by Single-grit

The surface of the workpiece that interferes with a grit is also conical as that of a grit. When the grit moves forward, a thrust force perpendicular to the workpiece surface is generated on the grit. The thrust force can be decomposed into a tangential force, a normal force and an axial force. Since the axial force is ignorable in surface grinding, only the normal and tangential forces of single-grit are considered as follows.

The engagements of a grit with the workpiece are described by three successive stages during cutting process [8], as given in Figure 2. In the first stage, the grit comes in contact with the workpiece and this leads to the only elastic deformation of the materials in the interfered area without the formed chip. In the second stage, the stress by the thrust force exceeds the yield strength of the workpiece materials, the grit penetrates into the workpiece, and the material is plastically ploughed to the front and to the sides of the grit without the formed chip. At the third phase, the grit penetrates into the workpiece with a critical depth of h_{cr} to form a chip; this critical cutting depth h_{cr} relates to the grit geometry, cutting conditions, and material properties of the workpiece.

Accordingly, the cutting force of single-grit is composed of two parts, i.e., cutting force for chip removal and frictional force to sustain a relative motion of the grinding wheel. Furthermore, the cutting force can be divided into a ploughing force and a cutting force for chip formation. The normal and tangential components of the single-grit cutting force can be expressed as

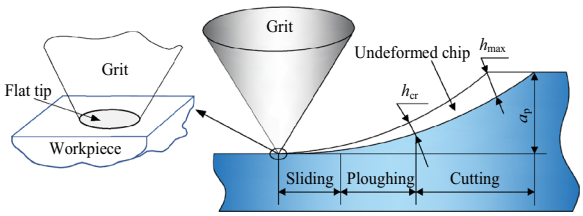

Figure 2 Engagement model of a grit and workpiece at three stages

$$f_n = f_{nf} + f_{np} + f_{nc}, \tag{11}$$

$$f_t = f_{tf} + f_{tp} + f_{tc}, \tag{12}$$

where f_n and f_t are the normal and tangential components of the cutting force of single-grit, respectively. f_{nf}, f_{np} and f_{nc} are the normal components of the friction, ploughing and cutting forces, respectively. f_{tf}, f_{tp} and f_{tc} are the tangential components of the friction, ploughing and cutting forces, respectively.

The tip area of the grit rubs on the workpiece without material removal; however, energy is consumed to overcome the friction force. The tip area of the grit is initially obtained in the dressing before cutting. As the cutting progress proceed, the tip area is gradually enlarged due to wear and tear, and the friction force is related to the worn area of the grit. Therefore, the normal and tangential components of the friction force are expressed as

$$f_{nf} = A\,\overline{P}, \tag{13}$$

$$f_{tf} = \mu A \overline{P}, \tag{14}$$

where μ is the friction coefficient between the workpiece and the grit; A is the tip area of the grit; $\overline{P}$ is the average contact pressure between the workpiece and the tip area of the grit. The lubrication state in the grinding zone during wet grinding is very complex. The friction coefficient is closely related to the properties, flow and injection angle of the coolant. It is difficult to establish the corresponding theoretical model of the grinding force. Therefore, both the theoretical models of grinding force and grinding experiments were performed in dry grinding.

The parabolic function is used to approximate the cutting path in a cutting process. Let the grinding wheel has a radius of $d_s/2$, and the cutting path has a curvature of R_1, the degree of non-conformity of the grinding wheel and the cutting path can be defined by a curvature difference Δ as [31]

$$\Delta = \frac{2}{d_s} - \frac{1}{R_1}. \tag{15}$$

Since the velocity of the workpiece is much slower than that of the grinding wheel, Eq. (15) can be further simplified as

$$\Delta = \pm \frac{4v_w}{d_e v_s}, \tag{16}$$

where d_s is the diameter of the grinding wheel; d_e is the equivalent diameter of the grinding wheel. The plus and minus signs represent the up-grinding and down-grinding, respectively.

With a significant curvature difference between the grinding wheel and the cutting path, the average contact pressure $\overline{P}$ is high to maintain the contact of the tip area of the grit with the workpiece. $\overline{P}$ is determined by the curvature difference (Δ) as [31].

$$\overline{P} = \Delta \cdot P_0 = \pm \frac{4v_w \cdot P_0}{d_e v_s}. \tag{17}$$

Substituting Eq. (17) into Eqs. (13) and (14) get the normal and tangential components of the friction force as

$$F_{nf} = \frac{4A \cdot v_w \cdot P_0}{d_e v_s}, \tag{18}$$

$$F_{tf} = \mu \frac{4A \cdot v_w \cdot P_0}{d_e v_s}, \tag{19}$$

where P_0 is a proportionality constant.

As the grit penetrates into the workpiece gradually, the workpiece material is continuously squeezed. When the cutting depth of the grit is lower than the critical cutting depth h_{cr}, the contact stress is below the yield strength of the workpiece material. The critical condition of grit action from sliding to ploughing is that the cutting depth of the grit is equal to h_{cr}. When the cutting depth of the grit is larger than h_{cr}, the workpiece materials are yielded and stacked at two sides of the grit, and the corresponding force is referred to a ploughing force.

In the grinding process, the grits indent the workpiece generating some plastic deformation, like the Brinell hardness test. The grits then move in the horizontal direction. This horizontal movement pushes the plastically deformed zone in the front of grits and shears the material and produces chips–acting as an extrusion process. The load in the Brinell test can be calculated as [8]

$$F_b = k_f \frac{HB \cdot \pi D}{2}\left(D - \sqrt{D^2 - d_1^2}\right), \tag{20}$$

where HB is the Brinell hardness of the workpiece material. The dynamic factor k_f is an empirical constant to be adjusted with experimental data. This factor lumps together the unmodeled phenomena such as thermal effects, imperfect grit geometry, and the difference between Brinell hardness number and dynamic hardness test. d_1 is the diameter of the impression given by $d_1 = D\sin(\theta)$. θ is the effective attack angle which is determined by chip thickness h and the affective diameter D of the grit as

$$\theta = \arccos(1 - 2h/D). \tag{21}$$

Accordingly, the normal and tangential components of the ploughing force are calculated as [8]

$$f_{np} = F_b(\cos\theta - \mu\sin\theta), \tag{22}$$

$$f_{tp} = F_b(\sin\theta + \mu\cos\theta). \tag{23}$$

The cutting force is calculated as the product of the chip cross-sectional area and the force coefficient. Assuming the chip has a circular cross-section as shown in Figure 1, the normal and tangential components of the cutting force by a single-grit are found as

$$f_{nc} = k_n E(A_{ch}) = \frac{\pi}{2} k_n E\left(h^2\right), \tag{24}$$

$$f_{tc} = k_t E(A_{ch}) = \frac{\pi}{2} k_t E\left(h^2\right), \tag{25}$$

where k_t and k_n are two constant coefficients for the normal and tangential cutting forces, respectively.

2.3 Grinding Force by Orderly-micro-grooved Wheel

The grits in the grinding zone can be divided into sliding, ploughing, and cutting grits according to their cutting depth, as shown in Figure 3.

The total grinding force by an orderly-micro-grooved wheel is the sum of all grinding forces by the active engaging grits in the grinding zone. It can be estimated as the multiplication of the single-grit grinding force and the number of active grits in the grinding zone as

$$F_t = N_{d1} f_t = N_{d1}\left(f_{tc} + f_{tp} + f_{tf}\right), \tag{26}$$

$$F_n = N_{d1} f_n = N_{d1}\left(f_{nc} + f_{np} + f_{nf}\right), \tag{27}$$

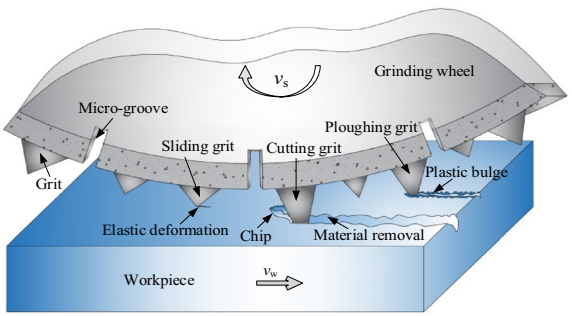

Figure 3 Three interaction states between grits and workpiece

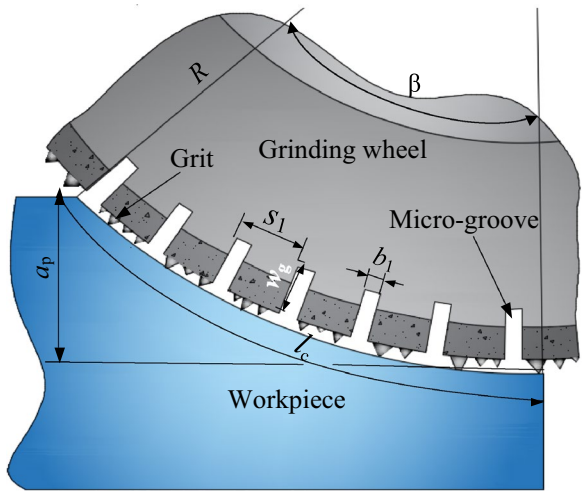

Figure 4 Contact zone between the workpiece and orderly-micro-grooved wheel

where F_t and F_n are the tangential and normal components of the total grinding force, respectively.

Macroscopically, the grinding wheel can be considered as a thick circular plate, and it is pressed against a curved surface of the workpiece in the grinding process, as shown in Figure 4. A large number of micro-grooves are distributed on the working surface of an orderly-micro-grooved grinding wheel, and no grits are crossed over the micro-grooves. Therefore, the number of active grits in the grinding zone of a micro-grooved wheel is smaller than that of a conventional wheel under the same grinding conditions. The number of active grits on an orderly-micro-grooved wheel is expressed as

$$N_{d1} = \alpha_n N_d, \tag{28}$$

where N_d and N_{d1} are the numbers of the active grits on a traditional and an orderly-micro-grooved grinding wheel, respectively. N_d is determined in Eq. (5) as $N_d = bl_cC_d$; α_n is the intermittent ratio of the orderly-micro-grooved wheel determined by the size of the micro-grooves as

$$\alpha_n = \frac{\pi d - nb_1}{\pi d}, \tag{29}$$

where n is the number of micro-grooves; b_1 is the width of the micro-groove, and d is the diameter of the grinding wheel.

The arc length of actual wheel-workpiece contact l_c can be calculated as

$$l_c = \frac{\beta}{2\pi} \times 2\pi R = R\beta, \tag{30}$$

$$\beta = \arccos\frac{R - a_p}{R}, \tag{31}$$

where β is the grinding wheel angle corresponding to the arc length of actual contact, and R is the radius of the grinding wheel.

Variable C_d depends on the dynamic effects, and it is also governed by the interaction force of the wheel and the workpiece as

$$C_d = C_0(\tan\varepsilon)^\tau, \tag{32}$$

$$\tan\varepsilon = \frac{v_w}{v_s}\left(\frac{a_p}{d_e}\right)^{1/2}, \tag{33}$$

where C_0 is the static grit density; τ is constant; ε is the infeed angle.

Concluding the aforementioned analysis, the tangential and normal components of the total grinding force by the orderly-micro-grooved grinding wheel can be derived as

$$F_t = b\alpha_n RC_0\left[\frac{v_w}{v_s}\left(\frac{a_p}{d_e}\right)^{1/2}\right]^\tau \arccos\left(\frac{R - a_p}{R}\right) \times \left[\frac{\pi}{2}k_t E\left(h^2\right) + F_b\left(\sin\theta + \mu_p\cos\theta\right) + \frac{4\mu A v_w P_0}{d_e v_s}\right], \tag{34}$$

$$F_n = b\alpha_n RC_0\left[\frac{v_w}{v_s}\left(\frac{a_p}{d_e}\right)^{1/2}\right]^\tau \arccos\left(\frac{R - a_p}{R}\right) \times \left[\frac{\pi}{2}k_n E\left(h^2\right) + F_b\left(\cos\theta - \mu_p\sin\theta\right) + \frac{4A v_w P_0}{d_e v_s}\right]. \tag{35}$$

2.4 Prediction of Grinding Force

Due to the powerful numerical computing function of Matlab, the force prediction model by Eqs. (34) and (35)

Table 1 Specifications of orderly-micro-grooved grinding wheel

Parameters	Value
Wheel diameter d (mm)	200
Wheel width b (mm)	4
Wheel type	Electroplated grinding wheel
Grit material	CBN
Number of micro-grooves n	600
Micro-groove width b_1 (mm)	0.1
Micro-groove depth w_g (mm)	1.5
Spacing of micro-grooves s_1 (mm)	1.05

Table 2 Grinding parameters in experiments

Parameters	Value
Grinding depth a_p (μm)	10, 15, 20, 25, 30, 35, 40
Workpiece velocity v_w (m/min)	2, 3, 4, 5, 6, 7
Wheel velocity v_s (m/s)	31.4

was programmed in this software, and it was used to calculate the normal and tangential components as well as the total grinding force subjected to the grinding conditions specified in Tables 1 and 2. Figure 5 shows the results of the total grinding force and each component forces. It indicates that the total grinding force equals the sum of cutting, ploughing, and frictional forces (Additional file 1).

With an increase of the grinding depth, both the number N_{d1} of active grits and the cutting depth of individual grit are increased in the grinding zone, and this results in the increases of cutting, ploughing and frictional forces significantly. Therefore, both the tangential and normal components of the grinding force are increased when the grinding depth is increased, as shown in Figure 5a and b. Moreover, the cutting force contributes the most to the total grinding force and its change with the grinding

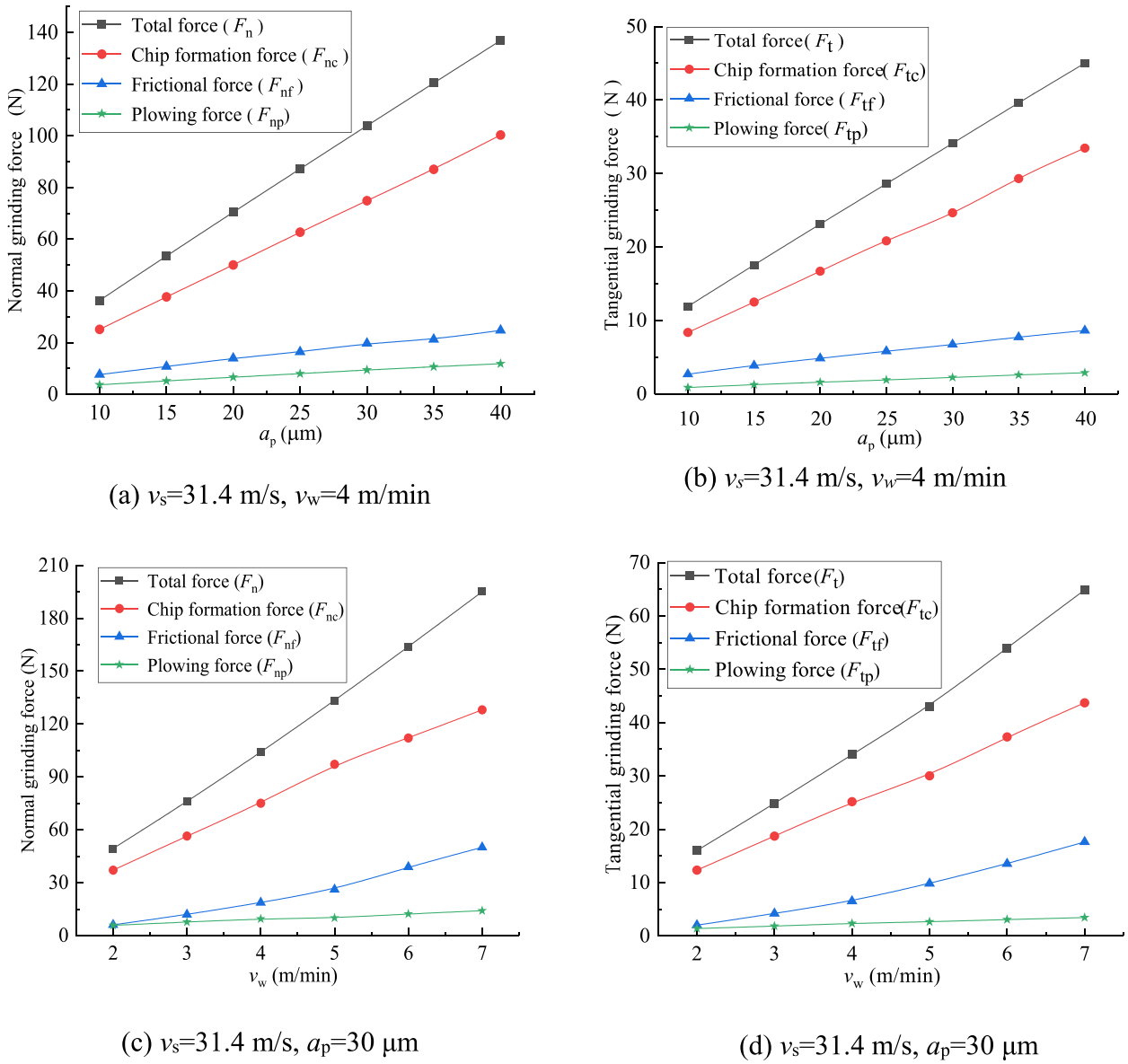

Figure 5 Predictions of grinding forces at different conditions

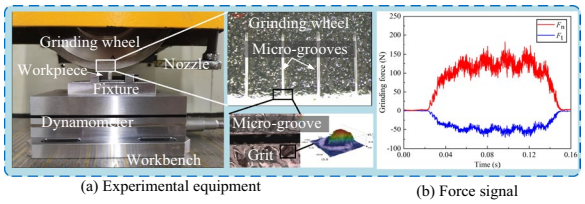

(a) Experimental equipment (b) Force signal

Figure 6 Setup of grinding experiments

depth is more obvious. It is understandable since workpiece materials are removed at the cutting stage.

With an increase of the feeding velocity of the workpiece, the number N_{d1} of active grits and the cutting depth of individual grit are changed slightly. The contribution of the cutting force to the total grinding force is still of most importance; however, its growth rate is reduced, as shown in Figure 5c and d. A significant increase of the friction force leads to the increase of normal and tangential components of the total grinding force.

3 Experimental Verification

3.1 Design of Experiments

To validate the proposed force prediction model, a number of surface grinding experiments of the electroplated wheel with orderly-micro-grooves were conducted on a high precision CNC grinding machine (MGK 7120×6, Hangzhou Machine Tool Co., Ltd., China). The experiments were carried out in dry grinding. Figure 6 shows the setup of grinding experiments. The workpiece material was hardened AISI 52100 with a hardness of 62± 0.5 HRC. The workpiece was cut into a length of 10 mm, a width of 10 mm and a height of 12 mm. The grinding method was down-grinding. Based on our previous studies [7], wider micro-grooves cause a larger vibration of the wheel, thus the grinding quality deteriorates. It is hard to fabricate micro-grooves with narrower widths. Therefore, the grinding wheel with 0.1 mm width micro-grooves was used to model and verify. Table 1 gives the structure and dimensions of the orderly-micro-grooved grinding wheel, and Table 2 specified the grinding parameters in experiments. Tables 3 and 4 show the chemical composition and the physical properties of AISI 52100, respectively. The grinding force was measured online by a 3-axis piezoelectric dynamometer (Kistler-9257B, Switzerland) with a sampling frequency of 5 kHz, The typical grinding force signal is shown in Figure 6. The grinding experiments were repetitively performed at least three times, and the measured grinding forces were averaged for the validation purpose. A comparative experiment was carried out using a traditional electroplated grinding wheel subjected to the same grinding conditions.

Table 4 AISI 52100 physical properties

Physical properties	Value
Elastic modulus (GPa)	208
Poisson's ratio	0.3
Density (g/cm^3)	7.8
Toughness(Nm/cm^2)	20
Tensile strength (MPa)	861.3
Yield strength (MPa)	518.42

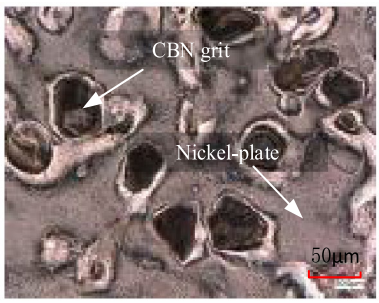

Figure 7 Distribution of grits on the orderly-micro-grooved grinding wheel

The grits on the working surface of the wheel were fall off and broke during grinding, and then a 3D ultra-depth of field microscope was used to observe the grits before the grinding experiment. Figure 7 shows the distribution of the grits and the static grit distribution density of the orderly-micro-grooved grinding wheel was 66 particles per square millimeter.

Table 3 AISI 52100 chemical composition

Alloying element (%)							
Cr	**Fe**	**Si**	**Mo**	**C**	**Mn**	**Ni**	**Cu**
≤1.65	≤0.30	≤0.35	≤0.10	≤0.10	≤0.05	≤0.30	≤0.25

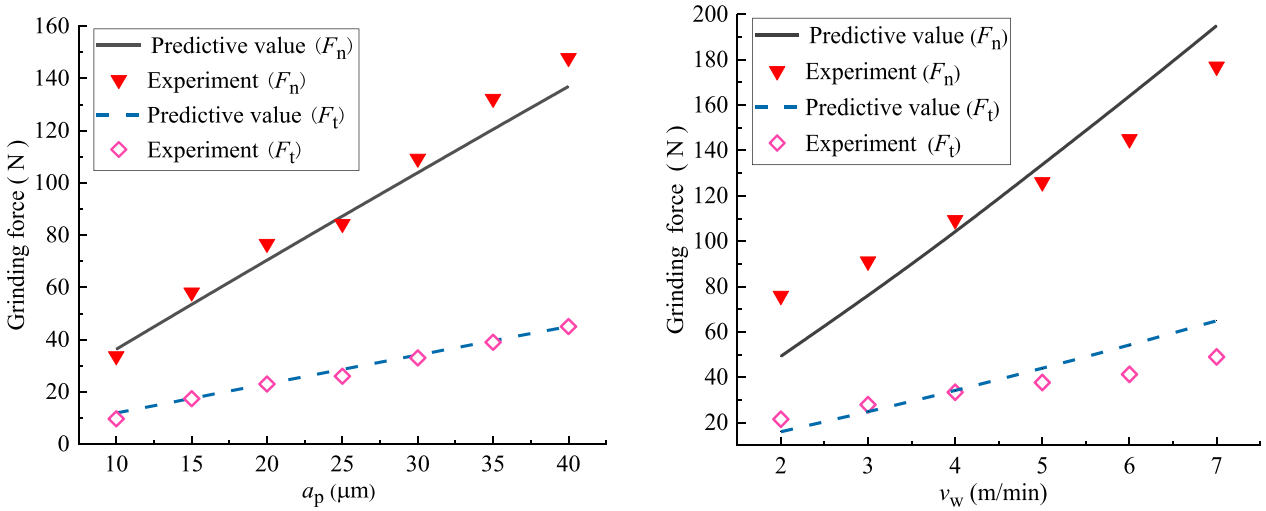

(a) v_s=31.4 m/s, v_w=4 m/min (b) v_s=31.4 m/s, a_p=30 μm

Figure 8 Comparison of predicted and measured grinding forces

3.2 Experimental Validation

Figure 8 presents the comparison of the predicted and measured grinding forces under different grinding conditions, and it shows a good agreement of the predicted forces with the measured forces in the experiments (Additional file 1). Figure 8a is for the comparison when the wheel velocity is 31.4 m/s and the workpiece velocity is 4 m/min; the average deviations in the percentage of the normal and tangential components at different grinding depths are 7.24% and 6.99%, respectively. As shown in Figure 8b, when the wheel velocity remains at 31.4 m/s and the grinding depth is set as 30 μm, the average deviations in the percentage of the normal and tangential components at different workpiece velocities are 16.7% and 18.27%, respectively. Moreover, it is clear that the influencing trends of the process parameters on the predicted forces are in good agreement with the trends reflected by the measured forces in the experiments.

4 Conclusions

This work was motivated by the authors' observation that even the grinding-force prediction was critical to control, monitor, and optimize a grinding process, no analytical model was available to predict grinding force by orderly-micro-grooved wheel. The authors aimed to develop a force-prediction model of hardened AISI 52100 by an electroplated grinding wheel with orderly-micro-grooves. The developed model was innovative in the sense that (1) a probabilistic function was adopted to represent random variants of undeformed chip thickness; note that the chip thickness affected greatly the grinding force; (2) a set of design variables including static grit density, and protruding heights and distribution density of grits were introduced to contemplate microstructure and characteristics of the orderly-micro-grooved grinding wheel explicitly.

To validate the reliability and effectiveness of the proposed model, surface grinding experiments were carried out and actual grinding forces subjected to different grinding conditions were measured for comparison. The validating results showed that the predicted grinding forces were in good agreement with the measured forces under the same grinding conditions; the influencing trends of main grinding parameters on the predicted force were consistent with the trends reflected by the measured forces in the experiments. The comparative study proved that the proposed analytical model was able to predict the grinding force by an orderly-micro-grooved wheel reliably. It is beneficial to understand the grinding mechanism, predict the grinding quality and optimize the grinding parameters.

Supplementary Information

The online version contains supplementary material available at https://doi.org/10.1186/s10033-023-00937-y.

Additional file 1. Table S1. Predictions of grinding forces at different conditions. **Table S2**. Comparison of predicted and measured grinding forces.

Acknowledgements
Not applicable.

Author Contributions
CM and MZ were in charge of the whole trial. CM and JW wrote the manuscript. XW, YL and ZMB gave some suggestions on the arrangement of the structure diagram and table in the paper. They also sorted out the relevant

references. WT, KT, YH and ZL put forward some suggestions on the thinking of the paper. All authors read and approved the final manuscript.

Authors' Information

Cong Mao, Born in 1975, is currently a Professor at *Hunan Provincial Key Laboratory of Intelligent Manufacturing Technology for High-performance Mechanical Equipment, Changsha University of Science and Technology, China*. He received PhD. degree from *Hunan University, China*, in 2008. His research interests include Precision processing technology of difficult-to-cut materials.

Jiali Wang, Born in 1996, is currently a master candidate at *Hunan Provincial Key Laboratory of Intelligent Manufacturing Technology for High-performance Mechanical Equipment, Changsha University of Science and Technology, China*.

Mingjun Zhang, Born in 1985, is currently an Associate Professor at *Hunan Provincial Key Laboratory of Intelligent Manufacturing Technology for High-performance Mechanical Equipment, Changsha University of Science and Technology, China*. He received PhD. degree on Mechanical Engineering from *Hunan University, China*, in 2013. His research interests include Precision processing technology of difficult-to-cut materials.

Xincheng Wang, Born in 1996, is currently an engineer at *Hunan Wuxin Intelligence Technology Co., Ltd, China*. He received his bachelor degree from *University of Washington, USA*, in 2019.

Yuanqiang Luo, Born in 1990, is currently a Lecturer at *Hunan Provincial Key Laboratory of Intelligent Manufacturing Technology for High-performance Mechanical Equipment, Changsha University of Science and Technology, China*. She received PhD. degree from *Hunan University, China*, in 2020.

Weidong Tang, Born in 1988, is currently a Lecturer at *Hunan Provincial Key Laboratory of Intelligent Manufacturing Technology for High-performance Mechanical Equipment, Changsha University of Science and Technology, China*. He received PhD. degree from *Shanghai Jiao Tong University, China*, in 2019.

Kun Tang, Born in 1980, is currently an Associate Professor at *Hunan Provincial Key Laboratory of Intelligent Manufacturing Technology for High-performance Mechanical Equipment, Changsha University of Science and Technology, China*. He received PhD. degree from *Hunan University, China*, in 2013.

Zhuming Bi, Born in 1965, is currently a Professor at *Department of Civil and Mechanical Engineering, Purdue University Fort Wayne, U.S.A*. He received PhD degree from *Harbin Institute of Technology, China*, in 1994.

Yongle Hu, Born in 1965, is currently a Professor at *Hunan Provincial Key Laboratory of Intelligent Manufacturing Technology for High-performance Mechanical Equipment, Changsha University of Science and Technology, China*. He received PhD. degree from *Zhejiang University, China*, in 2009.

Zhenheng Lin, Born in 1972, is currently a Professor at *College of School of Mechanical and Electrical Engineering, Putian University, China*. He received PhD. degree from *Xiamen University, China*, in 2010.

Funding

Supported by National Natural Science Foundation of China (Grant Nos. 52275405, 52275311, 51875050), Hunan Provincial Key Research and Development Program (Grant No. 2021GK2021).

Availability of data and materials statement

The data supporting the results in this study is available from the authors upon reasonable request.

Declarations

Competing Interests

The authors declare no competing financial interests.

Received: 3 August 2022 Revised: 18 August 2023 Accepted: 24 August 2023
Published online: 12 October 2023

References

[1] H N Li, D Axinte. Textured grinding wheels: a review. *International Journal of Machine Tools and Manufacture*, 2016, 109: 8-35.

[2] S Dewar, R Bauer, A Warkentin. Application of high-angle helical-grooved vitrified wheels to cylindrical plunge grinding. *International Journal of Advanced Manufacturing Technology*, 2018, 96(2): 2443-2453.

[3] L H Xu, Q Xu, J H Rao, et al. Experimental grinding of cubic zirconia with grooved and non-grooved diamond discs. *International Journal of Advanced Manufacturing Technology*, 2018, 97(5–8): 3087-3097.

[4] X H Zhang, Z C Zhang, Z H Deng, et al. Precision grinding of silicon nitride ceramic with laser macro-structured diamond wheels. *Optics & Laser Technology*, 2019, 109: 418-428.

[5} B Denkena, T Grove, T Go¨ttsching. Grinding with patterned grinding wheels. *CIRP Journal of Manufacturing Science and Technology*, 2014, 8: 12-21.

[6] B Kirsch, J C Aurich. Influence of the macro-topography of grinding wheels on the cooling efficiency and the surface integrity. *Procedia CIRP*, 2014, 13: 8-12.

[7] C Mao, P Long, W D Tang, et al. Simulation and experiment of electroplated grinding wheel with orderly-micro-grooves. *Journal of Manufacturing Processes*, 2022, 79: 284-295.

[8] R L Hecker, S Y Liang, X J Wu, et al. Grinding force and power modeling based on chip thickness analysis. *International Journal of Advanced Manufacturing Technology*, 2007, 33(5-6): 449-459.

[9] M Kadivar, B Azarhoushang, P Krajnik. Modeling of micro-grinding forces considering dressing parameters and tool deflection. *Precision Engineering*, 2021, 67: 269-281.

[10] Z L Ma, Q H Wang, H Chen, et al. A grinding force predictive model and experimental validation for the laser-assisted grinding (LAG) process of zirconia ceramic. *Journal of Materials Processing Technology*, 2022, 302: 117492.

[11] J Ni, K Feng, M S H Al-Furjan, et al. Establishment and verification of the cutting grinding force model for the disc wheel based on piezoelectric sensors. *Sensors*, 2019, 19(3): 725-738.

[12] H C Chang, J Wang. A stochastic grinding force model considering random grit distribution. *International Journal of Machine Tools and Manufacture*, 2008, 48(12-13): 1335-1344.

[13] S Agarwal, P Rao. Predictive modeling of force and power based on a new analytical undeformed chip thickness model in ceramic grinding. *International Journal of Machine Tools and Manufacture*, 2013, 65: 68-78.

[14] C W Dai, Z Yin, W F Ding, et al. Grinding force and energy modeling of textured monolayer CBN wheels considering undeformed chip thickness nonuniformity. *International Journal of Mechanical Sciences*, 2019, 157-158: 221-230.

[15] J Cheng, Y D Gong. Experimental study of surface generation and force modeling in micro-grinding of single crystal silicon considering crystallographic effects. *International Journal of Machine Tools and Manufacture*, 2014, 77: 1-15.

[16] C Li, X L Li, Y Q Wu, et al. Deformation mechanism and force modelling of the grinding of YAG single crystals. *International Journal of Machine Tools and Manufacture*, 2019, 143: 23-37.

[17] U Durgumahanti, V Singh, P V Rao. A new model for grinding force prediction and analysis. *International Journal of Machine Tools and Manufacture*, 2010, 50(3): 231-240.

[18] D V Ardashev, A A Dyakonov. Mathematical model of the grinding force with account for blunting of abrasive grains of the grinding wheel. *Journal of Manufacturing Science and Engineering*, 2017,139(12): 121005.

[19] M H Liu, X M Zhang, S C Xiu. Grinding force model for low-speed grinding based on impact principle. *Advanced Materials Research*, 2013, 797: 123-128.

[20] Y B Zhang, C H Li., H J Ji, et al. Analysis of grinding mechanics and improved predictive force model based on material-removal and plastic-stacking mechanisms. *International Journal of Machine Tools and Manufacture*, 2017,122: 81-97.

[21] G Y Sun, L L Zhao, Z Ma, et al. Force prediction model considering material removal mechanism for axial ultrasonic vibration-assisted peripheral grinding of Zerodur. *International Journal of Advanced Manufacturing Technology*, 2018, 98: 2775-2789.

[22] M Zhou, W Zheng. A model for grinding forces prediction in ultrasonic vibration assisted grinding of SiCp/Al composites. *International Journal of Advanced Manufacturing Technology*, 2016, 87: 9-12.

[23] Y L Xiao, S L Wang, C Ma, et al. Grinding force model for gear profile grinding based on material removal mechanism. *The International Journal of Advanced Manufacturing Technology*, 2023, 125: 743-762.

[24] X H Zhang, Z X Kang, S Li, et al. Grinding force modelling for ductile-brittle transition in laser macro-micro-structured grinding of zirconia ceramics. *Ceramics International*, 2019, 45(15): 18487-18500.
[25] X Z Xiao, K Zheng, W H Liao, et al. Study on cutting force model in ultrasonic vibration assisted side grinding of zirconia ceramics. *International Journal of Machine Tools and Manufacture*, 2016, 104: 58-67.
[26] H Jamshidi, E Budak. An analytical grinding force model based on individual grit interaction. *Journal of Materials Processing Technology*, 2020, 283: 116700.
[27] G Werner. Influence of work material on grinding forces. *Annals of CIRP*, 1978, 27: 243-248.
[28] J Y Tang, J Du, Y P Chen. Modelling and experimental study of grinding forces in surface grinding. *Journal of Materials Processing Technology*, 2008: 1-8.
[29] S Malkin, C Guo. *Grinding Technology: Theory and Application of Machining with Abrasives*. 2nd edition. New York: Industrial Press, 2008.
[30] E Budak, E Ozlu, H Bakioglu, et al. Thermo-mechanical modeling of the third deformation zone in machining for prediction of cutting forces. *CIRP Annals*, 2016, 65: 121-124.
[31] M C Shaw. *Principles of abrasive processing*. New York: Oxford University Press, 1996.